Microsecond Melting of a Folding Intermediate in a Coiled-Coil Peptide, Monitored by T-jump/UV Raman Spectroscopy†

Gurusamy Balakrishnan,‡ Ying Hu,‡,|| Martin A. Case,§ and Thomas G. Spiro*,‡

Department of Chemistry, Princeton University, Princeton, New Jersey 08544, and Department of Chemistry, The University of Vermont, Burlington, Vermont 05405

Received: March 30, 2006; In Final Form: May 22, 2006

A truncated version of the GCN4 coiled-coil peptide has been studied by ultraviolet resonance Raman (UVRR) spectroscopy with 197 nm excitation, where amide modes are optimally enhanced. Although the CD melting curve could be satisfactorily described with a two-state transition having T_m = 30 °C, singular value decomposition of the UVRR data yielded three principal components, whose temperature dependence implicates an intermediate form between the folded and unfolded forms, with formation and melting temperatures of 10 and 40 °C. Two α-helical amide III bands, at 1340 and 1300 cm^{-1}, melted out selectively at 10 and 40 °C, respectively, and are assigned to hydrated and unhydrated helical regions. The hydrated regions are proposed to be melted in the intermediate form, while the unhydrated regions are intact. Time-resolved UVRR spectra following laser-induced temperature jumps revealed two relaxations, with time constants of 0.2 and 15 μs. These are suggested to reflect the melting times of hydrated and unhydrated helices. The unhydrated helical region may be associated with a 14-residue "trigger" sequence that has been identified in the C-terminal half of GCN4. Dehydration of helices may be a key step in the folding of coiled-coils.

Introduction

GCN4 is a member of a large family of DNA binding proteins with a coiled-coil dimerization motif (Figure 1).[1−3] The coiled-coil involves two amphipathic α-helices, wound around each other and held together by hydrophobic interactions, which are additionally stabilized by electrostatic interactions of polar side chains. The sequences are characterized by heptad repeats of seven residues, **a** to **g**, with interacting apolar residues at **a** and **d** and complementary electostatic interactions at **e** and **g**.[4−7] These apolar residues are frequently leucines, and the interaction domain is characterized as a "leucine zipper".

GCN4 has been studied intensively as a simple model for the association of two polypeptide chains to form a folded protein. It has an unstructured DNA binding domain and a 33 residue dimerization domain with a C-terminal leucine zipper.[8−11] Truncated segments also dimerize,[12] and a 14-residue "trigger" sequence has been found to be necessary for assembly.[13] Melting of the dimer is cooperative and has frequently been described as a two-state process, although careful analysis of thermal profiles and the use of multiple probes have revealed more than two states.[14−20] Folding of the peptide is rapid, and heterogeneity in the kinetics, occasioned by the monomer−dimer association process, can be circumvented by cross-linking either the N- or the C-termini.[3,17,21,22]

Understanding the dynamics of protein folding and unfolding requires access to processes that are more rapid than can be studied by mixing techniques. The laser temperature-jump (T-jump) method permits studies of thermally induced processes on time scales as short as nanoseconds.[23−29] This technique has been applied to peptides and proteins, using fluorescence,[30−35] IR,[36−41] and Raman[25,27−29,42] spectroscopy to monitor folding and unfolding. Ultraviolet resonance Raman (UVRR) spectroscopy is a versatile probe, providing simultaneous access to different structural elements via resonance enhancement of vibrations arising from UV chromophores, including aromatic residues, and the amide bonds.

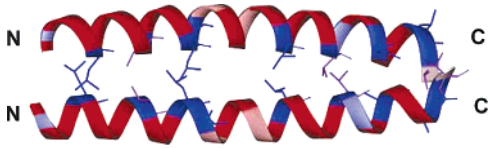

Figure 1. Ribbon diagram of the GCN4-p1 dimer.[1] The N and C termini are labeled with hydrophobic regions containing leucines (blue sticks), and valines (purple sticks) are highlighted in blue.

The melting of helices occurs on various time scales, depending on context. Unfolding times are on the order of hundreds of nanoseconds for short, hydrated helices but much longer in folded domains.[24,25,27,28,33,36,40,41] The melting dynamics of simple coiled-coils is of considerable interest in this context. Wang et al. have applied the T-jump/Fourier transform IR (FTIR) technique to cross-linked GCN4 and obtained relaxation times of 10 and 100 μs for helix melting, suggesting the presence of at least one intermediate between the folded and unfolded states.[22] In the present study, we examine a truncated version of GCN4, using T-jump/UVRR spectroscopy, and likewise detect two relaxations, but with much shorter time constants, 0.2 and 15 μs. In addition, the UVRR spectra permit detection of hydrated and unhydrated helical regions, which melt at greatly different temperatures, 10° and 40° C. The faster and slower relaxations are suggested to involve successive melting of these regions.

† Part of the special issue "Charles B. Harris Festschrift".

* To whom correspondence should be addressed. E-mail: spiro@princeton.edu. Tel: (609) 258 3907. Fax: (609) 258 0348.

‡ Princeton University.

§ The University of Vermont.

|| Current address: Department of Food Science, Cornell University, Ithaca, New York 14853.

10.1021/jp061987f CCC: $33.50
Published on Web 07/07/2006

Experimental Section

Materials. The nicotinamide derivative of a GCN4 model peptide (nic-GCN4-p23′) was synthesized on MBHA resin employing standard fmoc protocol using a multiple peptide synthesizer (ACT396, Advanced Chemtech). The side chains were deprotected with 100% TFA, and the peptide was cleaved from the resin using anhydrous HF with 10% anisole as scavenger. The peptide was purified by reverse-phase high-performance liquid chromatography (HPLC). The sequence of the nic-GCN4-p23′ peptide from the N- to C-terminus is as follows

Nicotinamide−GDKVEELLSKVWOLENEVARLKK−$CONH_2$

Nicotinamide was attached to the N-terminus for future metal ion-binding studies, the tyrosine (Y) to tryptophan (W) change provides a spectroscopic probe, and the C-terminus was amidated to avoid instability due to the charges at the terminus. The sequence includes a histidine (H) to ornithine (O) change to mitigate against interference from histidine in metal-binding experiments. Ornithine preserves the His−Glu salt bridge in the parent sequence. All other reagents were of analytical grade (Aldrich) and used as received. Aqueous solutions of nic-GCN4-p23′ peptides were prepared in 50 mM sodium phosphate buffer (pH 7.4) using Milli-Q Millipore water; 0.2 M $NaClO_4$ was added for the UVRR measurements.

Circular Dichroism. Far-UV circular dichroism spectra were measured with an AVIV 62DS spectropolarimeter equipped with a temperature-controlled cuvette holder, using a 1 mm quartz cell. The 4 °C CD spectra were averages of three repeated scans with 1 nm/s spacing from 300 to 190 nm. The temperature profiles were recorded at 222 nm from 1 to 80 °C with 1 °C/s steps and a 1 min equilibration time. A reverse scan, from 80 to 1 °C, was also carried out to verify reversibility. The peptide concentration was ∼0.2 mM (dimer). The data were converted to mean residue ellipticity [θ] in deg·cm^2/dmol using the equation = (θ_{obs}/10lc)/r, where θ_{obs} is the ellipticity measured in millidegrees, l is the optical path length (cm), c is the concentration of the peptide (M), and r is the number of residues. Secondary structure analyses of the CD spectra were carried out using the CONTINLL program in the CDPro software package.[43]

UV Raman Spectroscopy. The experimental setup has previously been described.[44] UV probe pulses (20 ns, 1 kHz) at 197 nm (∼1 μJ/pulse) were obtained by frequency quadrupling the output of a Ti:sapphire laser, which was pumped (527 nm, ∼10 mJ/pulse, 70 ns, 1 kHz) by an intracavity frequency-doubled Nd:YLF laser (GM30, Photonics International, Inc.). Raman scattered light was collected at 135° geometry and focused into a 1.26 m spectrograph (Spex 1269), which was equipped with a holographic grating (3600 groove/mm) and an intensified photodiode array detector (IPAD) (Roper Scientific). About 5 mL of the peptide (0.5 mM in dimer) solution was circulated through a wire-guided free-flowing cell to minimize decomposition and background scattering. Temperature control of the sample was achieved with a water bath (RTE-100, Neslab), which regulates the temperature of the sample cell and reservoir. UVRR spectra were collected with a 10 min accumulation time.

The UVRR spectra were frequency calibrated using the Raman spectrum of cyclohexane, and 0.2 M ClO_4^- was used as an internal intensity standard. Spectral analyses were carried out using GRAMS AI (Themo Electron Corp., formerly Galactic Industries) and Matlab (Mathworks, Natick, MA) platforms.

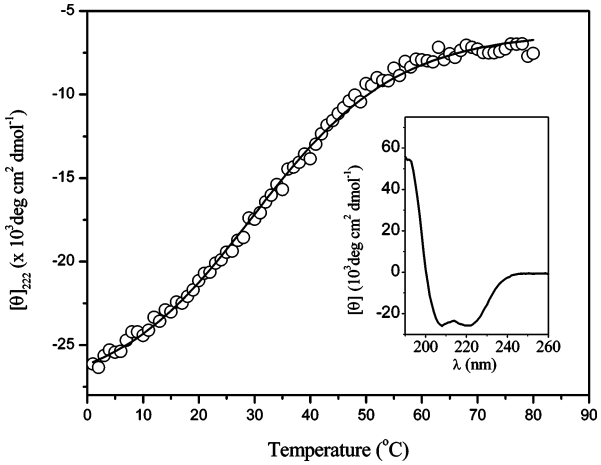

Figure 2. Thermal profile of the 222 nm ellipticity (θ_{222}) of nic-GCN4 (0.4 mM/monomer) associated with helical content. The continuous line is the fit to eq 1. The 4 °C CD spectrum (inset) shows the expected α-helical features. The goodness-of-fit parameter, R^2, was ∼0.999.

T-jump/Time-resolved UV Raman Measurements. The experimental setup and the spectral acquisition scheme have previously been described.[29] UV probe pulses for time-resolved UVRR measurements were generated by the UV laser described above. T-jump pulses were obtained from an intracavity diode laser-pumped Nd:YLF laser optical parametric oscillator (OPO; Photonics International, Inc.), which can generate tunable near-infrared (NIR) pulses at 1.6−2.0 μm (0.8−1.0 mJ/pulse, 20 ns, 1 kHz pulses). The final temperature of the sample after the T-jump was determined with a precision of 2 °C from the ∼3400 cm^{-1} water Raman band intensity change.[25,29] The frequency of the T-jump pump pulse is within the near-IR water band centered at 1.9 μm. The final temperature of the sample within the laser interaction volume is achieved instantaneously after the T-jump pulse (complete thermalization is reached within 10−20 ns). The probe and pump pulse sequence was alternated to minimize artifacts from spectrometer drift and photoproduct accumulation.[45] The timing between T-jump and probe pulses was adjusted with a computer-controlled pulse generator (DG 535, Stanford Research Systems). The final pump-probe (with T-jump) and probe-only (without T-jump) spectra were the averages over 10 min of accumulation.

Results

CD Temperature Profile. The far-UV CD spectra of nic-GCN4-p23′ at 4 °C (inset in Figure 2) show two negative bands, at 208 and 222 nm, characteristic of α-helices. Analysis of this spectrum with the CONTINLL program[43] yielded a helix fraction of 0.68. The temperature profile of the CD signal at 222 nm was modeled as a two-state helix-coil transition (Figure 2). The mean residue ellipticities at 222 nm, θ_{222}, which are linearly related to the mean helix content, were fit to the equation[46]

$$\theta_{222} = (\theta_H - \theta_C)/(1 + K_{eq}) + \theta_C \quad (1)$$

where K_{eq} is the equilibrium constant for unfolding and θ_H and θ_C are the baseline ellipticities for helix and the random coil states. The temperature-dependent equilibrium constant, K_{eq}, was calculated via

$$K_{eq} = \exp(-\Delta G/RT) \quad (2)$$

$$\Delta G = \Delta H + \Delta C_p(T - T_m) - T[\Delta S + \Delta C_p \ln(T/T_m)] \quad (3)$$

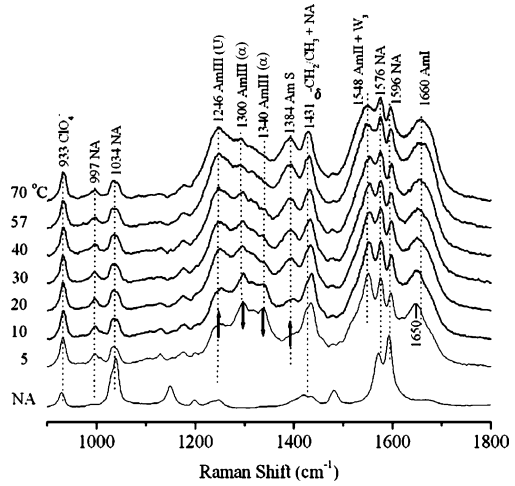

Figure 3. 197 nm excited UVRR spectra of nic-GCN4 (0.5 mM/dimer in 50 mM sodium phosphate buffer at pH 7.4 in the presence of 0.2 M sodium perchrolate) at several temperatures, with indicated band assignment. The bottom spectrum is of aqueous nicotinamide (2 mM in 50 mM sodium phosphate buffer at pH 7.4 in the presence of 0.2 M sodium perchrolate). (α = α-helix, U = unordered, NA = nicotinamide).

where T_m is the thermal melting temperature and ΔH, ΔS, and ΔC_p are the enthalpy, entropy, and heat capacity changes, respectively. The best fit (Figure 2) yields the following thermodynamic parameters: $T_m = 30$ °C, $\Delta H = 14.4$ kcal mol^{-1}, $\Delta S = 48$ cal K^{-1} mol^{-1}, and $\Delta C_p = 73$ cal K^{-1} mol^{-1}. The T_m is substantially lower than values reported for full-length GCN4,[12,18,22] reflecting the destabilizing effect of truncation and also of electrostatic repulsion between the nicotinamide groups, which are protonated at pH 7.

Although the data are satisfactorily fit ($R^2 = 0.998$) by this standard two-state treatment, they do not exclude the more complex scheme dictated by the UVRR measurements (below), since the transition is broad and the CD spectra are of low resolution.

UVRR Temperature Profile. Much higher resolution is available from UVRR spectra, which contain numerous bands, from several structural elements in the molecule (Figure 3). The spectra were obtained in the deep-UV region, with excitation at 197 nm, where optimal enhancement is observed for several amide modes,[44,47] which are sensitive to secondary structure. Amide I, which is mainly C═O stretching in character, shifts from 1650 cm^{-1} in α-helices to ∼1660 cm^{-1} in "unordered" structures.[47] ("Unordered" in this context simply means melted α-helix; there is considerable evidence that melting leads to a local conformation which is similar to the polyproline II (PPII) conformation.)[47−53] This shift is apparent in the nic-GCN4-p23′ UVRR spectra as the temperature is raised from 5 to 70 °C (Figure 3). Amide II, at 1548 cm^{-1}, does not change its frequency significantly but is more strongly enhanced in unordered structures.[47] However, it is overlapped with a tryptophan band, W3, which is expected to lose intensity at elevated temperature.[27] Consequently, the temperature profile of this band is uninformative (Figure 3). There are several components to the amide III mode, which has contributions from several coordinates, mainly C−N and C−C stretching and N−H and $C_α$−H bending.[54] Amide III depends strongly on peptide conformation. The main component is at 1246 cm^{-1} for the unordered structure; this band grows steadily as nic-GCN4-p23′ is heated. In contrast, the two bands assigned to the α-helix, 1300 and 1340 cm^{-1}, lose intensity at higher temperature. Finally, the amide S band, at 1384 cm^{-1}, is seen only for

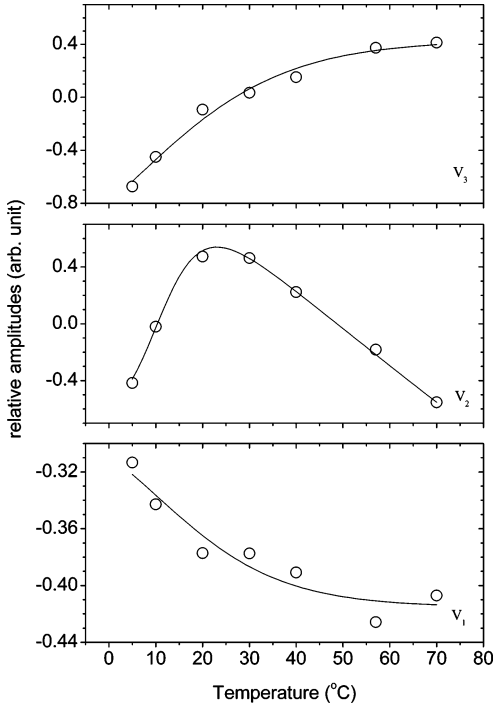

Figure 4. Amplitudes of the three principal components required to account for the temperature variation of the UVRR spectra. The continuous lines are the fit to the single (V_1 and V_3) and double (V_2) sigmoidal functions.

nonhelical structures.[55,56] It has significant $C_α$−H bending character, but this coordinate is thoroughly mixed into other modes at the α-helical conformation, for which no amide S is seen. This band approaches baseline at the lowest temperatures in the nic-GCN4-p23′ UVRR spectrum.

The nicotinamide substituent contributes several bands to the UVRR spectra (Figure 3, bottom), which are weakly temperature sensitive. In addition, there is an unusually strong band at 1431 cm^{-1}, which has some nicotinamide contribution but likely arises from side chain C−H bending coordinates. nic-GCN4-p23′ contains a high proportion of lysine and leucine residues, which contain a large number of CH_2 and CH_3 groups. They can contribute to the Raman intensity, even though side chain C−H bending is not expected to be enhanced via resonance with the amide electronic transitions.

To capture the full informational content of the complex UVRR spectra, we resorted to singular value decomposition (SVD)[57] of the entire set of spectra at seven different temperatures. Three principal components were required to account for most of the variation. Their amplitudes are plotted against temperature in Figure 4. V_1 decreases and V_3 increases with temperature, while V_2 reaches a maximum at an intermediate temperature. The increase of V_3 and decrease of V_1 are fitted with single sigmoidal functions, which results in a T_m value of 37 °C. The double sigmoidal functional fitting of the V_2 amplitude gives T_m values of 10 and 40 °C. We interpret this behavior to mean that nic-GCN4-p23′ has an intermediate as well as a folded and an unfolded state.

A three-state model, F ⇌ I ⇌ U, was constructed and used to compute fractional abundance (Figure 5), using the Boltzmann equation

$$f_i(T) = f(T_i) + \left[\frac{f(T_i) - f(T_f)}{1 + \exp\left(\frac{T - T_m}{\Delta T}\right)}\right] \qquad (4)$$

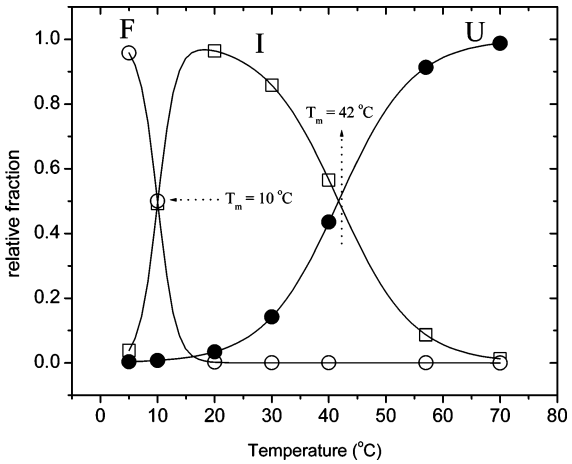

Figure 5. Population profiles for the folded (F), intermediate (I), and unfolded (U) forms of nic-GCN4 from SVD-based modeling of the UVRR spectra. The continuous lines are the fit to the single (F and U) and double (I) sigmoidal functions.

where f_i is the fractional population of the state "i" at a given temperature T, $f(T_i)$ and $f(T_f)$ are the fractional spectral intensities at the initial and final temperatures, and ΔT is the transition width. The total population at any temperature is given as

$$\Sigma f_{total}(T) = f_F(T) + f_I(T) + f_U(T) = 1 \quad (5)$$

Where $f_F(T)$, $f_I(T)$, and $f_U(T)$ are the fractional populations of the folded, intermediate, and unfolded states, respectively.

For the folded state, $f(T_i) = 1$ and $f(T_f) = 0$

$$f_F(T) = \left[1 + \exp\left(\frac{T - T_{m1}}{\Delta T_1}\right)\right]^{-1} \quad (6)$$

For the unfolded state, $f(T_i) = 1$ and $f(T_f) = 0$

$$f_U(T) = -\left[1 + \exp\left(\frac{T - T_{m2}}{\Delta T_2}\right)\right]^{-1} \quad (7)$$

and

$$f_I(T) = 1 - f_F(T) - f_U(T) \quad (8)$$

The T_m values (10 and 40 °C) and ΔT values (1.8 and 6.5 °C) are taken from the above fitting of the SVD amplitudes. This treatment assumes temperature independence for the spectra of the three states. The folded state (F) was found to convert entirely to the intermediate (I) state, with a transition temperature of 10 °C, and I converted to the unfolded state (U), with a 40 °C transition temperature. These temperatures bracket the 30 °C T_m of the CD melting profile (Figure 2), which clearly represents a weighted average of the two transitions detected by the UVRR spectra.

Finally, we used the three-state model parameters to extract UVRR spectra representative of each state (Figure 6). The F and U spectra have the characteristics expected for α-helices and unordered structures, respectively: amide I at 1648 and 1660 cm^{-1}, respectively, and the main amide III bands at 1300 and 1340 cm^{-1} for F but at 1250 cm^{-1} for U. Amide S, at 1384 cm^{-1}, is strong for U and absent for F. The spectrum of I is intermediate in character. Amide S and the 1246 cm^{-1} amide III band are about half as strong as in U, and the amide I frequency is at an intermediate value, 1652 cm^{-1}.

Interestingly, however, the spectrum of I discriminates between the two α-helical amide III bands. The 1300 cm^{-1} band

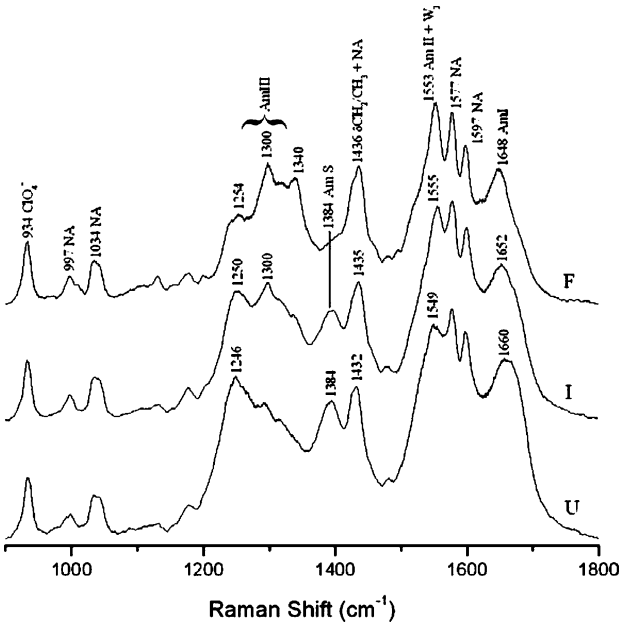

Figure 6. UVRR spectra of the F, I, and U forms of nic-GCN4, computed from the modeled populations (Figure 5).

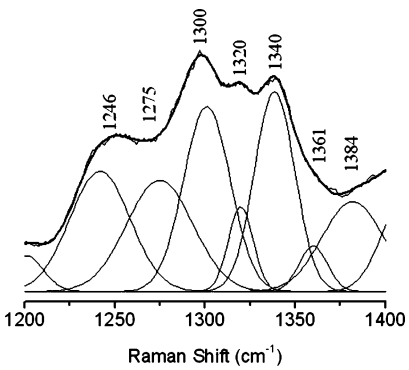

Figure 7. Example of UVRR band deconvolution, showing the quality of the data (thin line) and the fitting (thick line). The goodness-of-fit parameter, R^2, was ~0.998 at all temperatures.

is nearly as strong as it is in F, while the 1340 cm^{-1} band is greatly diminished. To investigate this difference, we deconvoluted these bands, as well as the 1246 and 1384 cm^{-1} bands associated with unordered structure using a minimal number of Gaussian bands. The quality of the data and of the fitting for the amide III and amide S regions (1200−1400 cm^{-1}) is illustrated in Figure 7. The deconvoluted band intensities were plotted against temperature (Figure 8). There is a striking correspondence with the three-state temperature profiles (Figure 5). The 1246 and 1384 cm^{-1} bands both show two stages of melting, with T_m values of ~10° and ~40 °C, consistent with the three-state analysis. The 1340 cm^{-1} band, however, melts out completely at quite low temperature, with a T_m of ~10 °C, while the 1300 cm^{-1} band melts only at higher temperature, with a T_m of ~40 °C. Thus, the 1340 cm^{-1} band disappears when F converts to I, while the 1300 cm^{-1} band disappears when I converts to U; both conversions increase the intensity associated with unordered structure.

This is the first observation of differential behavior for the 1300 and 1340 cm^{-1} amide III bands. Although both are associated with α-helices,[47] they must arise from structurally distinct units. The most likely structural difference is the presence or absence of H-bonding from solvent water. Hydrated

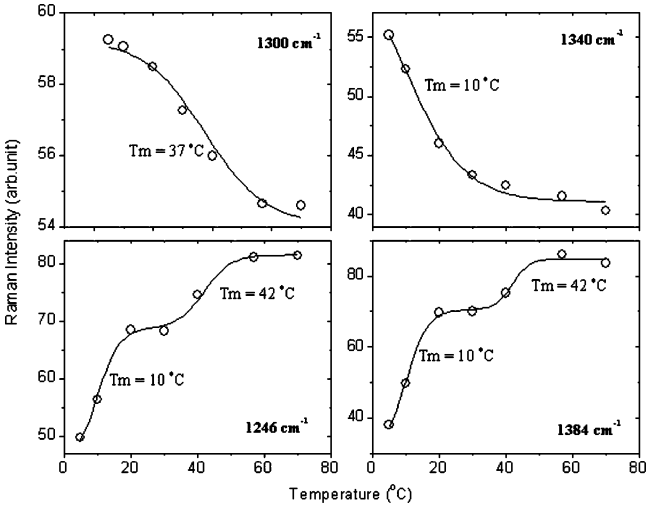

Figure 8. Thermal profiles of the peak heights of the marked bands, deconvoluted from the UVRR spectra. The continuous lines are the fit to the single (1300 and 1340 cm^{-1}) and double (1250 and 1394 cm^{-1}) sigmoidal functions.

and unhydrated α-helices have been distinguished by IR spectroscopy.[41,58,59] The former have amide I′ (the prime refers to the measurement being made in D_2O) at distinctly lower positions than the latter, ∼1635 vs ∼1650 cm^{-1}. It is not entirely clear why this behavior has not been observed in UVRR spectra; perhaps the lower frequency hydrated helix amide I mode is weakly enhanced. However, we note that Barron and co-workers have assigned a 1340 cm^{-1} band in the Raman optical activity spectrum to a hydrated α-helix.[60] This coincides with the low-melting 1340 cm^{-1} band in the nic-GCN4-p23′ UVRR spectra, which we therefore likewise assign to hydrated helical units. This assignment implies that, in the F structure, a portion of the helix is hydrated and that this portion melts upon forming I, which retains the unhydrated helical portion; the latter melts out only in U.

Time-resolved T-jump UVRR Spectra. Figure 9 shows UVRR spectra obtained before and after a T-jump and the evolution of the pump−probe difference spectrum in the nanosecond and microsecond regimes. The early time experiments utilized a 4°−32 °C T-jump, to capture the F to I transition (Figure 5), while the later time experiments utilized a 10−38 °C T-jump, to emphasize the I to U transition. At later times, there is a clear evolution toward the equilibrium 40 °C minus 10 °C difference spectrum, which is shown for comparison. The 1246, 1384, and 1660 cm^{-1} bands, all associated with unordered structure, increase monotonically with time.

Figure 10 shows time courses for the 1246 cm^{-1} band, deconvoluted from the time-resolved spectra. Time constants of 0.2 and 15 μs are associated with the 4°−32 °C and 10°−38 °C T-jumps, respectively. We tentatively assign these to the F to I and I to U transitions, respectively. Attempts to confirm these assignments by deconvoluting the 1300 and 1340 cm^{-1} bands, which distinguish between F and I (Figure 8), were unsuccessful, owing to the weakness of these bands.

Discussion

The dimerization domain of GCN4 is a 33-residue peptide (GCN4-p1),[12,18,21] with a melting temperature of ∼60 °C, as determined by CD thermal profiles and differential scanning calorimetry. The 23-residue fragment employed in this study (termed nic-GCN4-p23′, a variant of the previously studied "GCN4-p21" peptide[12]) was chosen for its limited stability,

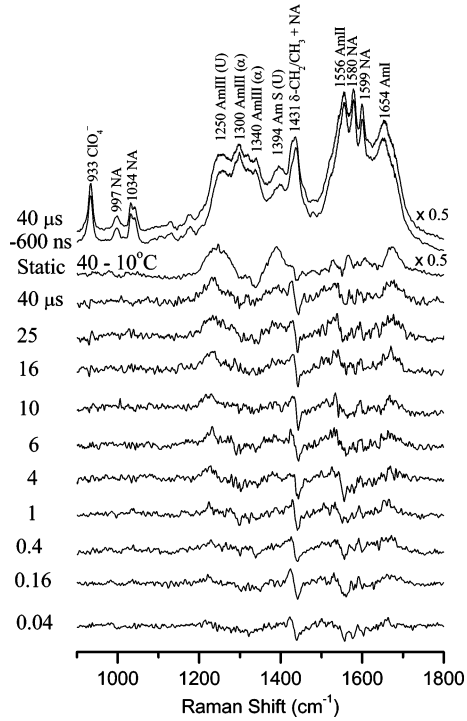

Figure 9. UVRR spectra before and after a 10−38 °C T-jump (top) and the equilibrium difference spectrum between 40° and 10 °C, toward which the pump−probe spectra evolve, following the T-jump; the early time data (<4 μs) were obtained with a 4−32 °C T-jump.

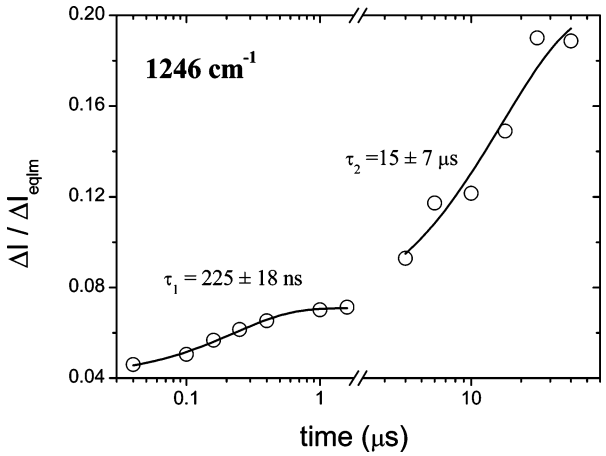

Figure 10. Time course of the 1245 cm^{-1} peak height, associated with unordered structure. The continuous lines are fit to a single-exponential function for the nanosecond (4−32 °C Δ*T*) and microsecond (10−38 °C Δ*T*) phases separately.

permitting access to substantial populations of folded and unfolded peptide over a convenient temperature range. (The nicotinamide substituent was added for later studies of stabilization by metal binding. In addition, ornithine was substituted for the single histidine residue in the wild-type sequence, which would also bind to metals, and tryptophan was substituted for the single tyrosine residue, as an additional spectroscopic probe.) Consistent with this aim, the CD melting temperature was reduced to 30 °C for nic-GCN4-p23′ (Figure 2).

Although the CD thermal profile of GCN4 peptides has frequently been fit to two-state melting behavior, it has become clear that the melting process proceeds through intermediate stages. Applying several techniques to GCN4-p1—CD, fluorescence, and heat capacity scanning calorimetry—Dragan and Privalov[18] were able to define three melting regimes, with transition temperatures ∼20, ∼50, and ∼70 °C. Wang[22] et al.

likewise found very different transition temperatures defined by fluorescence (~50 °C) and by CD or IR (~80 °C), for cross-linked GCN4-p1. The most direct evidence for intermediates was reported by Holtze et al.,[14] from multiple NMR resonances at intermediate temperatures for several residues.

In this study, we have established a stepwise melting process for nic-GCN4-p23′ from the temperature dependence of the UVRR spectra, whose multiple bands provide a rich source of structural information. Singular value decomposition of these spectra required three principal components, whose temperature dependence was that expected for an intermediate species between folded and unfolded states. Modeling of the spectra provided very different transition temperatures, 10 and 40 °C, for the formation and melting of this intermediate, which attains a large fractional population in between. These transitions were also observed as successive steps in the thermal profiles of the UVRR bands, 1246 and 1384 cm^{-1}, associated with formation of the unordered structure from the α-helix.

The UVRR spectra also provide the key to understanding the structural basis of these transitions. Two amide III bands associated with α-helical units, 1340 and 1300 cm^{-1}, diminish selectively at the two transition temperatures, 1340 cm^{-1} at 10 °C and 1300 cm^{-1} at 40 °C. This behavior requires that the two bands arise from α-helical units that are structurally distinct and that have very different melting behavior. A band at 1340 cm^{-1} is also the position of a Raman optical activity band which has been associated with hydrated α-helices. We therefore assign the Raman band to the same structural units. Hydrated helices have been detected in IR studies via a downshifted amide I′ band, ~1635 cm^{-1}, instead of the 1650 cm^{-1} position characteristic of unhydrated helices. The downshift results from the additional H-bonding from solvent molecules, which weakens the C═O bond. This has been established through selective ^{13}CO labeling of surface-exposed Ala residues and buried Leu residues for another GCN4 construct[58] and for a designed 3-helix bundle protein, α_3D.[59] The amide III frequency, which has a component of C−N stretching, tends to move oppositely to the amide I frequency,[61] since weakening of the C═O bond strengthens the amide C−N bond. Thus, it is reasonable that the amide III frequency of hydrated helices (1340 cm^{-1}) would be higher than that of unhydrated helices (1300 cm^{-1}). (However, the shift is substantially greater than that observed for amide I′, implying that other factors, perhaps involving altered torsion angles, must contribute.)

Thus, the UVRR spectra suggest that nic-GCN4-p23′ contains separate regions, in which the peptide bonds are predominantly hydrated or unhydrated and that the former melts at a much lower temperature than the latter. What might these regions be? Kammerer et al.[13] have identified a 14-residue "trigger" sequence, which seems to be required for coiled-coil formation in several proteins.[13] This sequence is a pair of heptads, but when it is substituted by arbitrary sequences which retain the leucine zipper motif, dimer formation is inhibited. The trigger sequence occurs in the C-terminal half of GCN4-p1 and of nic-GCN4-p23′. We hypothesize that the trigger sequence contains more unhydrated helix, because its intermolecular interactions are strong, and exclude the solvent, while the rest of the sequence, having weaker intermolecular interactions, contains more hydrated helix. In this scenario, the C-terminal region of nic-GCN4-p23′, containing the trigger sequence, would melt at 40 °C, while the N-terminal region would melt at 10 °C. The intermediate form would have melted N-terminal and unmelted C-terminal regions.

The time-resolved UVRR experiments showed two relaxations for nic-GCN4-p23′, following a T-jump, with time constants of 0.2 and 15 μs. Both were associated with a rise in unstructured peptide. The fast relaxation was obtained with a 4 to 32 °C T-jump, capturing the equilibrium transition from the folded to the intermediate state, while the slower relaxation was measured with a 10 to 38 °C T-jump, emphasizing the intermediate to unfolded transition. Thus, the 0.2 and 15 μs processes are suggested to reflect the melting of hydrated and unhydrated helices, respectively. Notably, the 0.2 μs relaxation is of the same order as the time constants reported for the melting of short monomeric α-helices in water.[25,34,41] We infer that the tightly bound portion of the peptide, presumably in the C-terminal half, melts more slowly than the loosely bound portion.

Wang et al.[22] likewise reported two time constants for the melting of the full length and cross-linked GCN4-p1′, 10 and 100 μs. If these relaxations arise from the same processes monitored by UVRR in nic-GCN4-p23′, then the order of magnitude slowing may be a reflection of the lower stability of nic-GCN4-p23′, relative to GCN4-p1′, due to the lack of cross-linking, the shorter sequence, and the presence of protonated nicotinamide in the former. Wang et al.[22] pointed out that the occurrence of an intermediate on the folding pathway is not inconsistent with apparent two-state folding, as observed in mixing experiments,[17,19,21,62,63] provided that the intermediate occurs after the main barrier to folding. The present results add a structural dimension to this perspective, since it seems likely that the folding barrier is associated with exclusion of water when tight contacts form. The formation of loosely bound hydrated helical units would be a post-barrier event.

Conclusions

This study presents the first clear evidence of differential melting of hydrated and unhydrated helices in a folded polypeptide chain. In the context of a coiled-coil structure, the hydrated regions melt at much lower temperature, no doubt reflecting the stability of the tightly bound regions from which water has been excluded. Time-resolved UVRR spectroscopy following a T-jump implicates fast melting for the hydrated regions and slower melting for the unhydrated regions. Dehydration of tight-binding regions is likely to be the rate-determining step in the folding of coiled-coil proteins.

Acknowledgment. This work was supported by NIH Grant GM 25158 to T.G.S. and NSF Award CHE 0106342 to M.A.C.

References and Notes

(1) Oshea, E. K.; Klemm, J. D.; Kim, P. S.; Alber, T. *Science* **1991**, *254*, 539.
(2) Weiss, M. A.; Ellenberger, T.; Wobbe, C. R.; Lee, J. P.; Harrison, S. C.; Struhl, K. *Nature* **1990**, *347*, 575.
(3) Oshea, E. K.; Rutkowski, R.; Kim, P. S. *Science* **1989**, *243*, 538.
(4) Crick, F. H. C. *Acta Crystallogr.* **1953**, *6*, 689.
(5) Lumb, K. J.; Kim, P. S. *Biochemistry* **1995**, *34*, 8642.
(6) Lee, D. L.; Ivaninskii, S.; Burkhard, P.; Hodges, R. S. *Protein Sci.* **2003**, *12*, 1395.
(7) Burkhard, P.; Stetefeld, J.; Strelkov, S. V. *Trends Cell Biol.* **2001**, *11*, 82.
(8) Dragan, A. I.; Frank, L.; Liu, Y. Y.; Makeyeva, E. N.; Crane-Robinson, C.; Privalov, P. L. *J. Mol. Biol.* **2004**, *343*, 865.
(9) Fujii, Y.; Shimizu, T.; Toda, T.; Yanagida, M.; Hakoshima, T. *Nat. Struct. Biol.* **2000**, *7*, 889.
(10) Keller, W.; Konig, P.; Richmond, T. J. *J. Mol. Biol.* **1995**, *254*, 657.
(11) Konig, P.; Richmond, T. J. *J. Mol. Biol.* **1993**, *233*, 139.
(12) Lumb, K. J.; Carr, C. M.; Kim, P. S. *Biochemistry* **1994**, *33*, 7361.

(13) Kammerer, R. A.; Schulthess, T.; Landwehr, R.; Lustig, A.; Engel, J.; Aebi, U.; Steinmetz, M. O. *Proc. Natl. Acad. Sci. U.S.A.* **1998**, *95*, 13419.
(14) Holtzer, M. E.; Lovett, E. G.; d'Avignon, D. A.; Holtzer, A. *Biophys. J.* **1997**, *73*, 1031.
(15) d'Avignon, D. A.; Bretthorst, G. L.; Holtzer, M. E.; Holtzer, A. *Biophys. J.* **1998**, *74*, 3190.
(16) d'Avignon, D. A.; Bretthorst, G. L.; Holtzer, M. E.; Holtzer, A. *Biophys. J.* **1999**, *76*, 2752.
(17) Moran, L. B.; Schneider, J. P.; Kentsis, A.; Reddy, G. A.; Sosnick, T. R. *Proc. Natl. Acad. Sci. U.S.A.* **1999**, *96*, 10699.
(18) Dragan, A. I.; Privalov, P. L. *J. Mol. Biol.* **2002**, *321*, 891.
(19) Wendt, H.; Baici, A.; Bosshard, H. R. *J. Am. Chem. Soc.* **1994**, *116*, 6973.
(20) Wendt, H.; Berger, C.; Baici, A.; Thomas, R. M.; Bosshard, H. R. *Biochemistry* **1995**, *34*, 4097.
(21) Krantz, B. A.; Sosnick, T. R. *Nat. Struct. Biol.* **2001**, *8*, 1042.
(22) Wang, T.; Lau, W. L.; DeGrado, W. F.; Gai, F. *Biophys. J.* **2005**, *89*, 4180.
(23) Ballew, R. M.; Sabelko, J.; Reiner, C.; Gruebele, M. *Rev. Sci. Instrum.* **1996**, *67*, 3694.
(24) Dyer, R. B.; Gai, F.; Woodruff, W. H. *Acc. Chem. Res.* **1998**, *31*, 709.
(25) Lednev, I. K.; Karnoup, A. S.; Sparrow, M. C.; Asher, S. A. *J. Am. Chem. Soc.* **1999**, *121*, 4076.
(26) Yamamoto, K.; Mizutani, Y.; Kitagawa, T. *Appl. Spectrosc.* **2000**, *54*, 1591.
(27) Huang, C. Y.; Balakrishnan, G.; Spiro, T. G. *Biochemistry* **2005**, *44*, 15734.
(28) JiJi, R. D.; Balakrishnan, G.; Hu, Y.; Spiro, T. G. *Biochemistry* **2006**, *45*, 34.
(29) Balakrishnan, G.; Hu, Y.; Spiro, T. G. *Appl. Spectrosc.* **2006**, *60*, 347.
(30) Ballew, R. M.; Sabelko, J.; Gruebele, M. *Proc. Natl. Acad. Sci. U.S.A.* **1996**, *93*, 5759.
(31) Snow, C. D.; Qiu, L. L.; Du, D. G.; Gai, F.; Hagen, S. J.; Pande, V. S. *Proc. Natl. Acad. Sci. U.S.A.* **2004**, *101*, 4077.
(32) Ervin, J.; Sabelko, J.; Gruebele, M. *J. Photochem. Photobiol., B* **2000**, *54*, 1.
(33) Hagen, S. J.; Eaton, W. A. *J. Mol. Biol.* **2000**, *301*, 1019.
(34) Thompson, P. A.; Eaton, W. A.; Hofrichter, J. *Biochemistry* **1997**, *36*, 9200.
(35) Rigler, R.; Rabl, C. R.; Jovin, T. M. *Rev. Sci. Instrum.* **1974**, *45*, 580.
(36) Huang, C. Y.; Klemke, J. W.; Getahun, Z.; DeGrado, W. F.; Gai, F. *J. Am. Chem. Soc.* **2001**, *123*, 9235.
(37) Colley, C. S.; Clark, I. P.; Griffiths-Jones, S. R.; George, M. W.; Searle, M. S. *Chem. Commun.* **2000**, 1493.
(38) Gulotta, M.; Rogatsky, E.; Callender, R. H.; Dyer, R. B. *Biophys. J.* **2003**, *84*, 1909.
(39) Reinstadler, D.; Fabian, H.; Backmann, J.; Naumann, D. *Biochemistry* **1996**, *35*, 15822.
(40) Gilmanshin, R.; Williams, S.; Callender, R. H.; Woodruff, W. H.; Dyer, R. B. *Proc. Natl. Acad. Sci. U.S.A.* **1997**, *94*, 3709.
(41) Williams, S.; Causgrove, T. P.; Gilmanshin, R.; Fang, K. S.; Callender, R. H.; Woodruff, W. H.; Dyer, R. B. *Biochemistry* **1996**, *35*, 691.
(42) Yamamoto, K.; Mizutani, Y.; Kitagawa, T. *Biophys. J.* **2000**, *79*, 485.
(43) Sreerama, N.; Woody, R. W. *Anal. Biochem.* **2000**, *287*, 252.
(44) Balakrishnan, G.; Hu, Y.; Nielsen, S. B.; Spiro, T. G. *Appl. Spectrosc.* **2005**, *59*, 776.
(45) Zhao, X. J.; Tengroth, C.; Chen, R. P.; Simpson, W. R.; Spiro, T. G. *J. Raman Spectrosc.* **1999**, *30*, 773.
(46) Becktel, W. J.; Schellman, J. A. *Biopolymers* **1987**, *26*, 1859.
(47) Huang, C. Y.; Balakrishnan, G.; Spiro, T. G. *J. Raman Spectrosc.* **2006**, *37*, 277.
(48) Mikhonin, A. V.; Myshakina, N. S.; Bykov, S. V.; Asher, S. A. *J. Am. Chem. Soc.* **2005**, *127*, 7712.
(49) Mikhonin, A. V.; Asher, S. A. *J. Phys. Chem. B* **2005**, *109*, 3047.
(50) Eker, F.; Griebenow, K.; Schweitzer-Stenner, R. *Biochemistry* **2004**, *43*, 6893.
(51) Eker, F.; Griebenow, K.; Cao, X. L.; Nafie, L. A.; Schweitzer-Stenner, R. *Proc. Natl. Acad. Sci. U.S.A.* **2004**, *101*, 10054.
(52) Asher, S. A.; Mikhonin, A. V.; Bykov, S. *J. Am. Chem. Soc.* **2004**, *126*, 8433.
(53) Schweitzer-Stenner, R.; Eker, F.; Kai, G. *Biophys. J.* **2004**, *86*, 341A.
(54) Krimm, S.; Bandekar, J. *Adv. Protein Chem.* **1986**, *38*, 181.
(55) Jordan, T.; Spiro, T. G. *J. Raman Spectrosc.* **1994**, *25*, 537.
(56) Wang, Y.; Purrello, R.; Jordan, T.; Spiro, T. G. *J. Am. Chem. Soc.* **1991**, *113*, 6359.
(57) Henry, E. R.; Hofrichter, J. *Methods Enzymol.* **1992**, *210*, 129.
(58) Manas, E. S.; Getahun, Z.; Wright, W. W.; DeGrado, W. F.; Vanderkooi, J. M. *J. Am. Chem. Soc.* **2000**, *122*, 9883.
(59) Walsh, S. T. R.; Cheng, R. P.; Wright, W. W.; Alonso, D. O. V.; Daggett, V.; Vanderkooi, J. M.; DeGrado, W. F. *Protein Sci.* **2003**, *12*, 520.
(60) McColl, I. H.; Blanch, E. W.; Hecht, L.; Barron, L. D. *J. Am. Chem. Soc.* **2004**, *126*, 8181.
(61) Wang, Y.; Purrello, R.; Georgiou, S.; Spiro, T. G. *J. Am. Chem. Soc.* **1991**, *113*, 6368.
(62) Sosnick, T. R.; Jackson, S.; Wilk, R. R.; Englander, S. W.; DeGrado, W. F. *Proteins: Struct., Funct., Genet.* **1996**, *24*, 427.
(63) Zitzewitz, J. A.; Bilsel, O.; Luo, J. B.; Jones, B. E.; Matthews, C. R. *Biochemistry* **1995**, *34*, 12812.